ACS APPLIED MATERIALS & INTERFACES

Research Article

www.acsami.org

Template-Free Synthesis of Ruthenium Oxide Nanotubes for High-Performance Electrochemical Capacitors

Ji-Young Kim,[†,§] Kwang-Heon Kim,[†] Hyun-Kyung Kim,[†] Sang-Hoon Park,[†] Kwang Chul Roh,[*,‡] and Kwang-Bum Kim[*,†]

[†]Department of Materials Science and Engineering, Yonsei University, 134 Shinchon-dong, Seodaemoon-gu, Seoul 120-749, Republic of Korea

[‡]Energy Efficient Materials Team, Energy and Environmental Division, Korea Institute of Ceramic Engineering and Technology, 101, Soho-ro, Jinju-si, Gyeongsangnam-do 660-031, Republic of Korea

Supporting Information

ABSTRACT: One-dimensional, hydrous ruthenium oxide nanotubes ($RuO_2 \cdot 1.84H_2O$) have been successfully achieved using a template-free, microwave-hydrothermal process. These were found to be amorphous in nature and have a large specific surface area of 250 $m^2 \cdot g^{-1}$, producing a specific and volumetric capacitance of 511 $F \cdot g^{-1}$ and 531 $F \cdot cm^{-3}$, respectively, at a discharging current density of 0.5 $A \cdot g^{-1}$. When used as an electrode material in an electrochemical capacitor or ultracapacitor, they produced a significant improvement in capacitance, rate capability, and cyclability that can be attributed to the hollow nature of tubes allowing greater contact between the active surface of the electrode and the electrolyte.

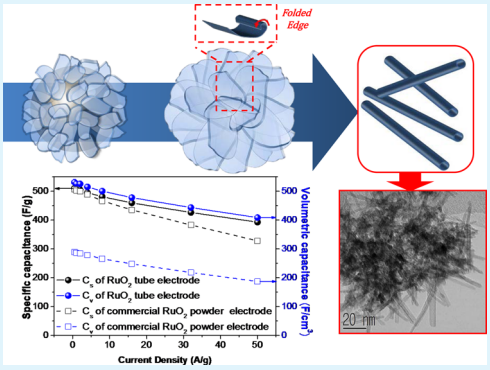

KEYWORDS: *electrochemical capacitors (or ultracapacitor), ruthenium oxide, template-free synthesis, nanotubes, electrochemical performance*

INTRODUCTION

The high charging/discharging rate, good stability, and long cycling life of electrochemical capacitors (otherwise known as supercapacitors or ultracapacitor or ECs)[1−7] makes them ideally suited for use as a power source for the memory backup of mobile devices or high-power applications such as hybrid electric vehicles. Depending on the particular charge storage mechanism used by an EC, there are two possible processes that can occur at the electrodes. The first of these is the electrical double layer capacitance which arises from the charge separation at the electrode/electrolyte interface. The second one is pseudocapacitance. In pseudocapacitors, the fast and reversible reactions take place.[5,8,9] In the case of the latter, the electrode is usually made from a conducting polymer or transition metal oxides;[10−16] however, ruthenium oxide ($RuO_2 \cdot xH_2O$), despite being expensive, tends to be the preferred option as it provides a high specific capacitance and high rate capability.

The electrochemical performance of an EC is highly dependent on the size and shape of its electrodes at a nanometer scale, making the design and fabrication of nanomaterials with a well-defined morphology of crucial concern.[17] Nanostructured materials such as zero-dimensional (0D) nanoparticles and one-dimensional (1D) nanotubes offer a means of achieving the high surface area and large surface-to volume ratio needed to allow effective contact with the electrolyte and sufficiently reduce the ion diffusion path to ensure rapid electron/ion transfer.[18,19] However, such particles also tend to be prone to agglomeration, which drastically reduces the surface-to-volume ratio and electrochemical utilization of the active material.[20] This has led to significant effort being directed toward the synthesis of metal oxide/carbon nanocomposites;[21−26] however, a potential limitation of such nanocomposites is the use of carbon for the synthesis, which lowers the volumetric capacitance and gravimetric (or specific) capacitance owing to its low density and low specific capacitance.[16,20] This is of particular significance in practical applications where space is a concern, as the volumetric capacitance and volumetric energy density in such cases are just as important, if not more, than the gravimetric energy density.[27] Despite this, supercapacitors are frequently classified as high performance based on their gravity capacitance rather than volumetric capacitance.

Clearly, any further enhancement of the electrochemical behavior of EC electrodes requires the rational design of electroactive materials with well-defined nanostructures.[28] To this end, the use of nanotubes offers a number of advantages in terms of offering greater packing density, electron transport

Received: May 20, 2015
Accepted: July 10, 2015
Published: July 10, 2015

DOI: 10.1021/acsami.5b04360
ACS Appl. Mater. Interfaces 2015, 7, 16686−16693

along the vertical axis, electrolyte access, and electrical contact without agglomeration; these ultimately lead to a higher rate capability and greater cyclic stability.[29−32] Of the various methods available for synthesizing nanotubes, solution-based chemical methods tend to provide the best combination of quality, quantity, and reproducibility.[33−38] Therefore, up until now, most 0D RuO_2 structures have been prepared by using either sol−gel or hydrothermal methods.[39] However, previous reports of RuO_2 nanotubes have relied on a template-based method that relies on anodic aluminum oxide (AAO) or manganese oxide nanorods and, therefore, requires additional steps to remove the template.[40] The development of a simple, template-free method of producing RuO_2 nanotubes is therefore of great interest to large-scale preparation and application.

In this study, we use a microwave-hydrothermal process to carry out, for the first time, the template-free synthesis of 1D RuO_2 nanotubes. We hope to produce EC electrodes with an improved gravimetric and volumetric capacitance, which would make them ideally suited for use in electrochemical capacitors. The mechanism behind the morphological evolution of these nanotubes[1−6] is discussed in relation to the effect this has on the capacitance and rate capability.

EXPERIMENTAL SECTION

Synthesis. Synthesis of the nanotubes was achieved by a microwave-hydrothermal process, in which 1.0 g of $RuCl_3{\cdot}nH_2O$ (Sigma-Aldrich) powder was first added to 100 mL of a 10 M NaOH aqueous solution (Sigma-Aldrich). This solution was then stirred at room temperature for 3 days, during which time a black precipitate was formed. Next, the solution and precipitate were transferred into a Teflon vessel, which was sealed and placed in a microwave system (MARS-5, CEM). This was then heated to 200 °C in less than 10 min and maintained at this temperature for 0.5, 2, or 4 h. Once the reaction was completed, the Teflon vessel was removed from the microwave system and cooled to room temperature. The resulting suspension was then filtered, and the residue collected was washed with water and freeze-dried.

Characterization. The morphology and structure of the nanotubes produced were characterized by transmission electron microscopy (TEM: JEM-3010, JEOL), X-ray diffraction (XRD: Rigaku, Cu Kα, 40 kV, 20 mA), and Raman spectroscopy (T64000, Jobin Yvon). X-ray photoelectron spectroscopy (XPS: Thermo Electron, ESCA 2000) was used to analyze elemental composition. Thermogravimetric experiments were carried out on a thermogravimetric analyzer (Mettler Toledo) in flowing air by increasing the temperature from room temperature to 800 °C at a rate of 10 °C·min^{-1}.

Electrochemical measurements were performed using a three-electrode electrochemical cell, in which a platinum plate and saturated calomel electrode were used as the counter and reference electrodes, respectively. The working electrode was fabricated from a mix of 75 wt % nanotubes, 15 wt % carbon black, and 10 wt % polyvinylidene fluoride dissolved in *N*-methylpyrrolidone. This slurry was coated onto a titanium foil and dried overnight at 80 °C. The area of the resulting working electrode was 1 × 1 cm^2 and contained approximately 1−2 mg of nanotubes. For comparison, the initial precipitate sample, RuO_2-120 min sample, and commercial $RuO_2{\cdot}H_2O$ nanopowder (Sigma-Aldrich) electrodes were also prepared with the same weight ratio of 75:15:10.

Cyclic voltammetry (CV) and charge/discharge testing was performed in a 1 M H_2SO_4 solution within a potential window of 0.0−1.0 V_{SCE} using a potentiostat/galvanostat (VMP3, Princeton Applied Research). The current response in the CV curves was normalized with respect to the mass of the nanotubes, while the total electrode weight and volume were used to calculate the specific capacitance (C_s) and volumetric capacitance (C_v), respectively. All current rates were set on the basis of the RuO_2 nanotube in the working electrode, allowing the volumetric capacitance to be calculated as

$$C_v(\mathrm{F{\cdot}cm^{-3}}) = C_s(\mathrm{F{\cdot}g^{-1}}) \times d(\mathrm{g{\cdot}cm^{-3}}) \quad (1)$$

where d is the typical density of the electrode. The density is calculated by dividing the mass with the volume of the electrode (area × thickness, measured).

RESULTS AND DISCUSSION

The black-colored precipitate produced by the addition of $RuCl_3{\cdot}nH_2O$ to NaOH was identified as $RuO_2{\cdot}2H_2O$, while the green supernatant was found to contain RuO_4^- anions due to the disproportionation reaction of ruthenate, RuO_4^{2-}, according to the redox potential−pH diagram.[17,41,42]

$$3RuO_4^{2-} + (2 + x)H_2O \rightarrow 2RuO_4^- + RuO_2{\cdot}xH_2O + 4OH^- \quad (2)$$

The precipitate was deemed to be amorphous because its XRD pattern lacked any discernible peaks, and so XPS analysis was used to determine its oxidation state. This revealed two peaks, one at 280.8 eV for Ru $3d_{5/2}$ and one at 285.5 eV for Ru $3d_{3/2}$, indicating the presence of RuO_2[43,44] (Figure S1a, Supporting Information). The diameter of this initially formed RuO_2 particle was 300−400 nm (Figure S1b,c, Supporting Information).

Microwave-hydrothermal treatment of the solution at 200 °C for 4 h produced 20−60 nm long nanotubes of RuO_2 with a diameter of ca. 5−7 nm, as shown in Figure 1a. The high

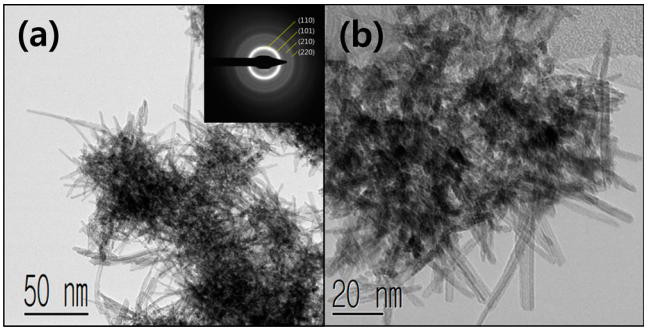

Figure 1. TEM images of ruthenium oxide nanotubes. (b) is a magnified image of (a) (Inset: selected area electron diffraction (SAED) of ruthenium oxide nanotubes).

magnification image in Figure 1b confirms the hollow nature of these tubes. In Figure 1, numerous one-dimensional products (nanotubes and nanorods) are observed and most of them are nanotubes. In the initial stage of the microwave-hydrothermal process, the nanosheets are generated on the surface of RuO_2 precipitates and from perruthenate (RuO_4^-) solution. We believe that the nanosheets grow with an increasing tendency of curling, leading to the formation of nanotubes. We will discuss the formation mechanism later. The nanotubes are entangled with each other, forming mesopores due to the formation mechanism of the nanotube. Fortunately, the high capacitance values can be obtained for mesoporous networks of entangled nanotubes with an open central channel. The inset of Figure 1a shows the corresponding selected area electron diffraction (SAED) pattern. The corresponding SAED patterns in Figure 1a confirm that these hierarchical architectures are polycrystalline.

The formation process of these nanotubes was investigated by varying the synthesis reaction time. Nanosheets were found

DOI: 10.1021/acsami.5b04360
ACS Appl. Mater. Interfaces 2015, 7, 16686−16693

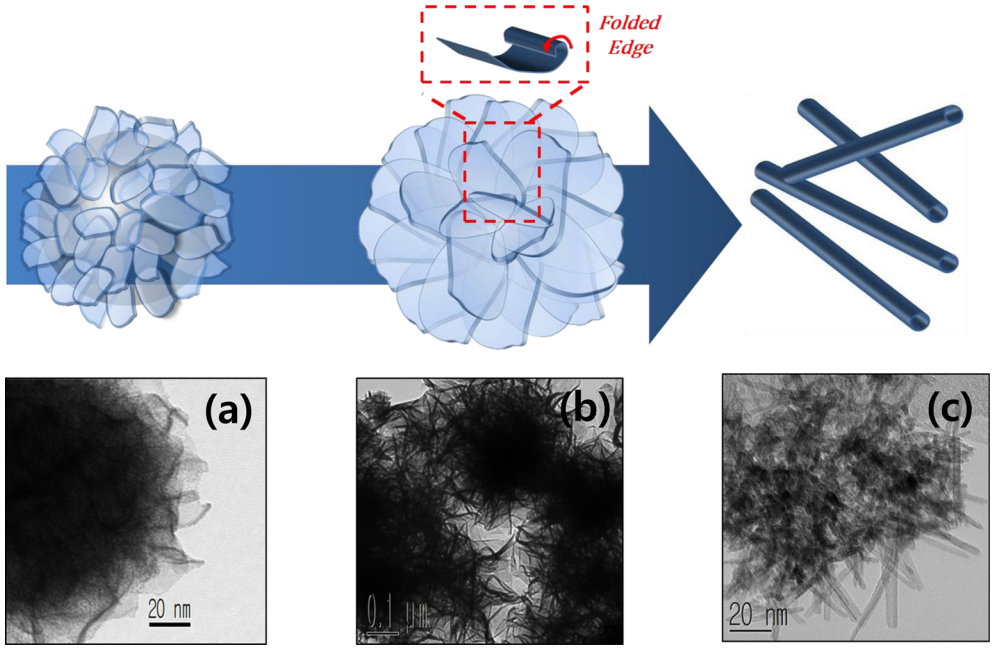

Figure 2. Schematic illustrating the proposed nanotube formation mechanism and TEM images of nanotubes formed for different reaction times: (a) reaction time = 0.5 h, (b) reaction time = 2 h, and (c) reaction time = 4 h.

to form on the surface of irregular particles within the first 0.5 h (Figure 2a); however, when the reaction time was increased to 2 h, nanoflowers composed of multiple nanosheets were formed (Figure 2b). The mechanism of the formation of different nanostructures with time has been proposed in a previous study.[41] Closer inspection of these nanoflowers reveals that they have a tendency to curl into tubes, and so as the reaction proceeds, more and more nanotubes are observed (Figure 3). These observations suggest that nanotube-like

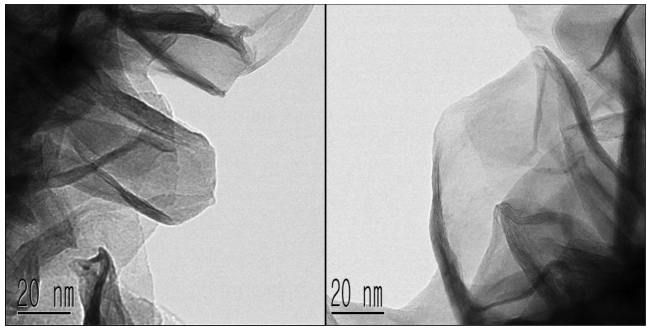

Figure 3. TEM images of curling sheets at the nanoflowers produced after 2 h of microwave-hydrothermal treatment.

products are first generated on the surface of RuO_2 precipitates during the initial stages of the hydrothermal reaction, though there are a number of possible mechanisms by which nanotubes could be formed from nanosheets. The mechanism considered most likely in this instance is shown in Figure 2. In this case, the driving force for rolling is provided by surface forces generated by localized regions of high surface energy and mechanical tension created by the high temperature and pressure of the process.[45] The exact mechanism for the formation of tubular nanostructures in our study is still under investigation. However, on the basis of our observations, we proposed the rolling mechanism for the conversion from nanosheets to nanotubes.

It is clear that the much more open structure of the RuO_2 nanotubes would allow faster H^+ ion diffusion, leading to an improved high rate capability when used as an EC electrode. This nanoscale structure also affords several other advantages, such as its 1D nature allowing for a substantially higher tap density by increasing the volumetric energy density.[46] For example, the tap density of RuO_2 nanotube powders is around 0.88 $g \cdot cm^{-3}$, while that of commercial RuO_2 powder is about 0.55 $g \cdot cm^{-3}$, making the former a more attractive candidate for the positive electrode in ECs designed for a high energy density. This concept of using a 1D nanostructure to maximize tap density has been demonstrated in the past with carbon, silicon, and various other materials.[47−49] The use of a 1D nanotube has also been shown in previous studies to reduce the tortuosity of electron and ion transport, thereby improving the rate capability.[50,51]

The X-ray diffraction (XRD) pattern of the RuO_2 nanotubes formed after 2 and 4 h (Figure 4a) reveals two broad, low-intensity peaks at 32° and 37° that are concordant with the (110) and (101) reflections of rutile RuO_2 (JCPDS No. 43-1027). As reaction time increased, we can observe that the intensity of peaks is slightly higher. The broadening of these peaks suggests that the sample is in a poorly crystalline state, and so, Raman spectroscopy was used to examine the microstructure further (Figure 4b). This identified only a single broad peak at 470 cm^{-1} attributable to hydrated RuO_2,[52−54] and so given the clearly nanocrystalline nature of the nanotubes, XPS was used to determine their composition. As can be seen in Figure 4c,d, this revealed Ru $3d_{5/2}$, Ru $3d_{3/2}$, and O 1s peaks at 281.2, 285.4, and 530.0 eV, respectively. This corresponds to the binding energy of Ru^{4+}, thus confirming the presence of RuO_2.[55,56]

Since the electrochemical properties of RuO_2 are highly dependent on its degree of hydration,[39] thermogravimetric analysis was performed to estimate the hydration number (x) of the $RuO_2 \cdot xH_2O$ present in the nanotubes formed after 4 h. The nanotubes exhibited a continuous weight loss of approximately

DOI: 10.1021/acsami.5b04360
ACS Appl. Mater. Interfaces 2015, 7, 16686−16693

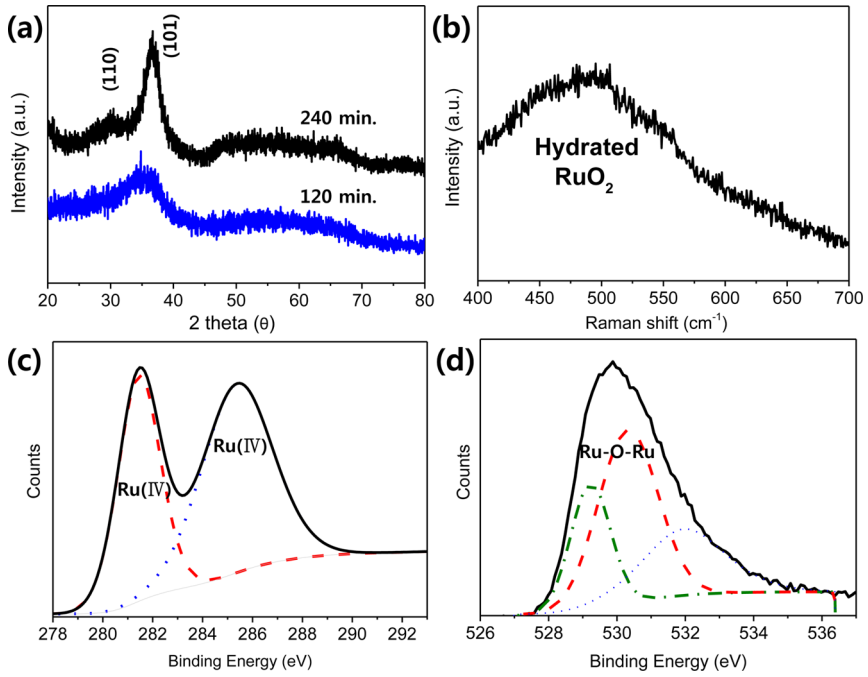

Figure 4. (a) XRD patterns, (b) Raman spectra, and (c) Ru 3d and (d) O 1s XPS spectra of nanotubes synthesized using a microwave-hydrothermal process.

20.0% of their initial weight (Figure S2, Supporting Information) up to 200 °C; from this, we determined the chemical composition to be $RuO_2 \cdot 1.84H_2O$.[57]

To further research the specific surface areas and the porous nature of RuO_2 nanostructures, nitrogen adsorption−desorption isotherms are shown in Figure S3, Supporting Information, and the inset illustrates the corresponding Barrett−Joyner−Halenda (BJH) pore size distribution plots. Subsequent measurements of the nanotubes produced a Type IV isotherm with H3 hysteresis. The morphology of the nanotubes resulted in a high BET surface area of approximately 250 $m^2 \cdot g^{-1}$, which is a value that is comparable to that of ruthenium oxide/carbon composites.[58] The average pore diameter was 3−4 nm, according to the BJH plot calculated from the nitrogen isotherms of the nanotubes. The pores may correspond to the pores inside the nanotubes. This result is in good agreement with the results of TEM, indicating the nanotubes are mainly formed. This is advantageous when it comes to enhancing the performance of an EC, as the combination of a large specific surface area and open tubular structure ensures a short ion diffusion path and rapid ion transport.[19]

To evaluate the electrochemical properties of an electrode based on the synthesized RuO_2 nanotubes (RuO_2-240 min samples), cyclic voltammograms (CVs) were measured within a 0.0−1.0 V_{SCE} potential window at various scan rates in 1 M H_2SO_4 to evaluate its rate capability. In the resulting CV curves (Figure 5a,b), the current has been normalized with respect to the mass of the electrode. Note that in Figure 5a only a single broad peak was obtained in both the anodic and cathodic scans, which is typical capacitive behavior of $RuO_2 \cdot xH_2O$ and indicates that the capacitance is produced by both a Faradaic mechanism and double-layer mechanism. The electrode exhibited a featureless CV for scan rates as high as 100 $mV \cdot s^{-1}$, indicating its superior high rate capability, which was because the electrolyte had greater access to the electrode's active surface.

In Figure 5b, the charge−discharge tests of synthesized RuO_2 nanotubes (RuO_2-240 min samples) performed at current densities of 0.5−50 $A \cdot g^{-1}$ also revealed that no significant voltage (IR) drop occurs at the beginning of the discharge cycle at densities between 0.5 and 16 $A \cdot g^{-1}$, suggesting that the electrical conductivity of the electrode is reasonably high. The specific capacitance of the electrode was calculated to be 511, 506, 505, 495, and 393 $F \cdot g^{-1}$ at discharge current densities of 0.5, 1, 2, 4, and 50 $A \cdot g^{-1}$, respectively, indicating a decrease in specific capacitance of only 23% over this current density range (black solid circles, Figure 5c). We investigated the electrochemical properties of materials prepared in a shorter reaction time, the initial precipitates, and RuO_2-120 min. The specific capacitances of initial precipitate and RuO_2-120 min sample were 337 and 501 $F \cdot g^{-1}$ at discharge current density of 0.5 $A \cdot g^{-1}$, respectively. The low specific capacitance of initial precipitates can be attributed to its large and irregular particle size. The specific capacitance of RuO_2-120 min sample is similar to that of RuO_2-240 min sample at low current density. However, the specific capacitances of initial precipitates and RuO_2-120 min sample were decreased rapidly, and the voltage (IR) drop increased with a higher discharging current density (Figure S4, Supporting Information). We cannot evaluate the specific capacitance initial precipitates and RuO_2-120 min sample over 8 and 16 $A \cdot g^{-1}$, respectively, due to its rapid drop. It suggests that the crystallinities of the initial precipitates and RuO_2-240 min sample were very poor and increased with an increase in the hydrothermal reaction time to 240 min. This observation is consistent with the results obtained from the XRD measurement, too (in Figure 4a).

The factors that contribute most to this high specific capacitance and good high-rate capability are the easy access to the interior afforded by the open ends of the nanotubes and the fast mass transport of H^+ ions to electrochemically active sites. The hydrous nature of the nanotubes may also play an

DOI: 10.1021/acsami.5b04360
ACS Appl. Mater. Interfaces 2015, 7, 16686−16693

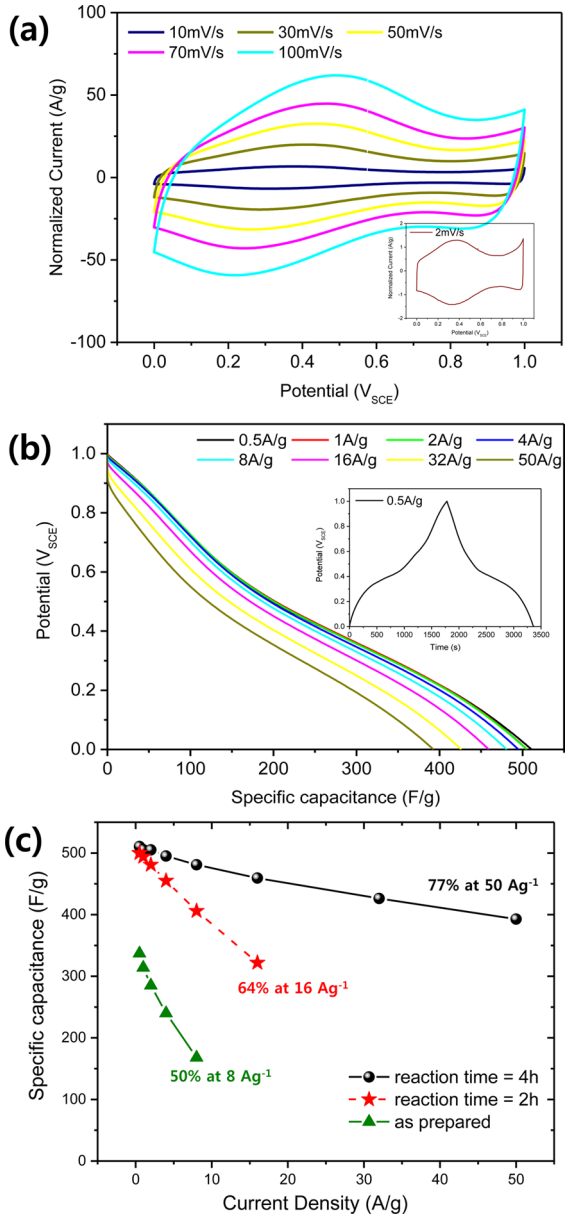

Figure 5. (a) Cyclic voltammograms (CVs) at scan rates of 10−100 $mV{\cdot}s^{-1}$ (inset: 2 $mV{\cdot}s^{-1}$). (b) Discharge curves (current density: 0.5−50 $A{\cdot}g^{-1}$) (inset: charge−discharge curve at 0.5 $A{\cdot}g^{-1}$) of RuO_2 nanotube electrode. (c) Specific capacitances of materials with different reaction times. Circles: RuO_2-240 min (RuO_2 nanotube) electrode; stars: RuO_2-120 min electrode; triangles: initial precipitate electrode.

important role, however, in promoting the mass transfer of protons and accelerating the redox transitions of RuO_2.

As the volumetric capacitance of an electrode is another critically important concern, the specific capacitances in Figure 6 were converted to volumetric capacitances based on an electrode density of 1.04 $g{\cdot}cm^{-3}$. This revealed that the volumetric capacitance of these nanotube electrodes can be as high as 531 $F{\cdot}cm^{-3}$ at 0.5 $A{\cdot}g^{-1}$, which is more than 1.8 times the value obtained with a commercial RuO_2 nanopowder electrode (289 $F{\cdot}cm^{-3}$ = 507 $F{\cdot}g^{-1}$ × ~0.57 $g{\cdot}cm^{-3}$). The right axis of Figure 6 shows the volumetric capacity of the RuO_2 nanotube electrode derived from the specific capacitance on the left axis. It can be seen that there is an increase in the

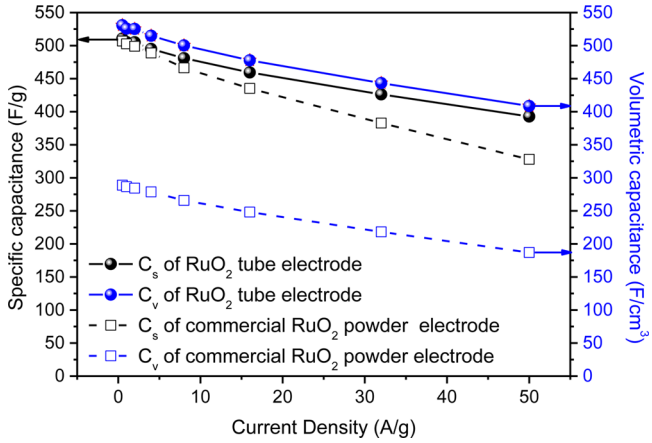

Figure 6. Specific (left) and volumetric (right) capacitances (circles: RuO_2 nanotube electrode; squares: commercial RuO_2 powder electrode).

volumetric capacitance over the gravimetric capacitance owing to the high tap density of the nanotube powder. Thus, although there are few references to the volumetric capacitance of RuO_2 in the literature, it is useful to note that the volumetric capacitance is comparable to the gravimetric capacitance.

The specific capacitance and high rate capability of RuO_2 electrodes have been found to be highly sensitive to the amount of water in the structure.[39,59] For example, when unannealed and containing at least two water molecules, RuO_2 has a specific capacitance of 527 $F{\cdot}g^{-1}$.[39] This value reaches a maximum of 720−900 $F{\cdot}g^{-1}$ when it is annealed at 150 °C to give an approximate composition of $RuO_2{\cdot}0.5H_2O$;[25] however, when measured at a scan rate of 50 $mV{\cdot}s^{-1}$, the specific capacitance decreases rapidly to just 36% of that measured at 2 $mV{\cdot}s^{-1}$. In addition, although hydrous RuO_2 with high capacitances of up to 1500 $F{\cdot}g^{-1}$ and excellent high rate capabilities have been reported, an accurate comparison is made difficult by the ultralight mass of these electrodes.[14,60]

A long cycle life is another critical factor to the practical application of EC electrodes, with Figure 7 showing the variation in specific capacitance of the nanotube electrode after repeated cycles at a constant scan rate of 50 $mV{\cdot}s^{-1}$. It is evident from this that even after 5000 cycles a superior capacitance retention of 88.5% was maintained. This is in stark

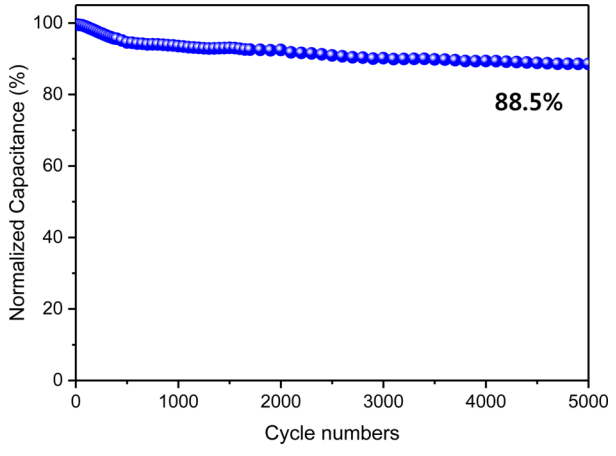

Figure 7. Cyclability of the nanotube electrode (at constant scan rate of 50 mV s^{-1}).

DOI: 10.1021/acsami.5b04360
ACS Appl. Mater. Interfaces 2015, 7, 16686−16693

contrast to previous reports, in which the capacitance of highly hydrous RuO_2 (hydration degree x = 2.0) dropped so rapidly that only 4% of its initial capacitance was maintained after 50 cycles.[15] Moreover, even though the cyclability of hydrous RuO_2 (hydration degree x = 0.5) improves after being heated to 150 °C, its loss of capacitance is still significant (45% after 200 cycles).

The high capacitance, excellent rate capability, and good cycling stability of RuO_2 nanotube electrodes can be attributed to both their hydrous nature and the high surface area created by their unique 1D hollow structure. The interior space created by the tubular nanostructure allows easy penetration of the electrolyte into both the inner region of the electrode and its outer surface area, resulting in reduced internal resistance and improved electrochemical performance.

CONCLUSIONS

The template-free synthesis of 1D-ruthenium oxide nanotubes has been made possible by the use of a microwave-hydrothermal process. This unique morphology has been shown to produce a greatly improved specific and volumetric capacitance, remarkable rate capability, and superior cycle performance when used as an electrode material in an electrochemical capacitor. This excellent electrochemical performance is attributed to the ease with which an electrolyte can access the interior of the tubes through their open ends, thereby ensuring the rapid mass transport of H^+ ions to electrochemically active sites. The hydrous nature of the nanotubes can also play an important role in promoting the mass transfer of protons and accelerating the redox transitions of RuO_2.

ASSOCIATED CONTENT

Supporting Information

S1: (a) XPS and (b) TEM images of initial precipitates before microwave-hydrothermal reaction and (c) a higher magnification image of (b); S2: thermogravimetric analysis (TGA) of nanotubes formed using a reaction time of 4 h; S3: N2 adsorption−desorption isotherms of the nanotubes formed using a reaction time of 4 h. The Supporting Information is available free of charge on the ACS Publications website at DOI: 10.1021/acsami.5b04360.

AUTHOR INFORMATION

Corresponding Authors

*E-mail: kbkim@yonsei.ac.kr. Fax: 82-2-312-5375. Tel: 82-2-365-7745 (K.-B. Kim).
*E-mail: rkc@kicet.re.kr (K. C. Roh).

Present Address

§Center for Energy Convergence Research, Green City Technology Institute, Korea Institute of Science and Technology (KIST), Hwarang-ro 14-gil 5, Seongbuk-gu, Seoul 136-791, Korea

Author Contributions

J.-Y.K., K.C.R., and K.-B.K. conceived, planned, and designed the experiments. J.-Y.K., K.-H.K., and H.-K.K. synthesized the cathode materials and performed TEM, XPS, BET, TGA, and electrochemical tests. S.-H.P. contributed to discussion of the Raman and XRD results. J.-Y.K. and K.C.R. wrote the main manuscript. K.C.R. and K.-B.K. supervised the whole process. All authors reviewed the manuscript.

Notes

The authors declare no competing financial interest.

ACKNOWLEDGMENTS

This work was supported by the energy efficiency and resources grant (No: 20122010100140 and No: 20122010100090) of the Korea Institute of Energy Technology Evaluation and Planning (KETEP) funded by the Ministry of Knowledge Economy, Korean government.

REFERENCES

(1) Simon, P.; Gogotsi, Y. Materials for Electrochemical Capacitors. *Nat. Mater.* **2008**, *7*, 845−854.
(2) Miller, J. R.; Simon, P. Electrochemical Capacitors for Energy Management. *Science* **2008**, *321*, 651−652.
(3) Deng, W. T.; Ji, X. B.; Chen, Q. Y.; Banks, C. E. Electrochemical Capacitors Utilising Transition Metal Oxides: An Update of Recent Developments. *RSC Adv.* **2011**, *1*, 1171−1178.
(4) Hou, Y.; Cheng, Y. W.; Hobson, T.; Liu, J. Design and Synthesis of Hierarchical MnO_2 Nanospheres/Carbon Nanotubes/Conducting Polymer Ternary Composite for High Performance Electrochemical Electrodes. *Nano Lett.* **2010**, *10*, 2727−2733.
(5) Ramirez-Castro, C.; Crosnier, O.; Athouël, L.; Retoux, R.; Bélanger, D.; Brousse, T. Electrochemical Performance of Carbon/MnO_2 Nanocomposites Prepared via Molecular Bridging as Supercapacitor Electrode Materials. *J. Electrochem. Soc.* **2015**, *162*, A5179−A5184.
(6) Liu, S.; Sun, S.; You, X. Z. Inorganic Nanostructured Materials for High Performance Electrochemical Supercapacitors. *Nanoscale* **2014**, *6*, 2037−2045.
(7) Kim, I. H.; Kim, K. B. Ruthenium Oxide Thin Film Electrodes Prepared by Electrostatic Spray Deposition and Their Charge Storage Mechanism. *J. Electrochem. Soc.* **2004**, *151*, E7−E13.
(8) Conway, B. E. *Electrochemical Supercapacitors: Scientific Fundamentals and Technological Applications*; Kluwer Academic/Plenum Press: New York, 1999.
(9) Brousse, T.; Bélanger, D.; Long, J. W. To Be or Not To Be Pseudocapacitive? *J. Electrochem. Soc.* **2015**, *162*, A5185−A5189.
(10) Frackowiak, E.; Béguin, F. Carbon Materials for the Electrochemical Storage of Energy in Capacitors. *Carbon* **2001**, *39*, 937−950.
(11) Wang, Y. G.; Li, H. Q.; Xia, Y. Y. Ordered Whiskerlike Polyaniline Grown on the Surface of Mesoporous Carbon and Its Electrochemical Capacitance Performance. *Adv. Mater.* **2006**, *18*, 2619−2623.
(12) Toupin, M.; Brousse, T.; Bélanger, D. Charge Storage Mechanism of MnO_2 Electrode Used in Aqueous Electrochemical Capacitor. *Chem. Mater.* **2004**, *16*, 3184−3190.
(13) Sugimoto, W.; Iwata, H.; Yasunaga, Y.; Murakami, Y.; Takasu, Y. Preparation of Ruthenic Acid Nanosheets and Utilization of Its Interlayer Surface for Electrochemical Energy Storage. *Angew. Chem., Int. Ed.* **2003**, *42*, 4092−4096.
(14) Hu, C. C.; Chang, K. H.; Lin, M. C.; Wu, Y. T. Design and Tailoring of the Nanotubular Arrayed Architecture of Hydrous RuO_2 for Next Generation Supercapacitors. *Nano Lett.* **2006**, *6*, 2690−2695.
(15) Jang, J. H.; Kato, A.; Machida, K.; Naoi, K. Supercapacitor Performance of Hydrous Ruthenium Oxide Electrodes Prepared by Electrophoretic Deposition. *J. Electrochem. Soc.* **2006**, *153*, A321−A328.
(16) Kim, J. Y.; Kim, K. H.; Park, S. H.; Kim, K. B. Microwave-Polyol Synthesis of Nanocrystalline Ruthenium Oxide Nanoparticles on Carbon Nanotubes for Electrochemical Capacitors. *Electrochim. Acta* **2010**, *55*, 8056−8061.
(17) Li, G. R.; Xu, H.; Lu, X. F.; Feng, J. X.; Tong, Y. X.; Su, C. Y. Electrochemical Synthesis of Nanostructured Materials for Electrochemical Energy Conversion and Storage. *Nanoscale* **2013**, *5*, 4056−4069.
(18) Wu, D.; Liu, J.; Zhao, X. N.; Li, A. D.; Chen, Y. F.; Ming, N. B. Sequence of Events for the Formation of Titanate Nanotubes,

DOI: 10.1021/acsami.5b04360
ACS Appl. Mater. Interfaces 2015, 7, 16686−16693

Nanofibers, Nanowires, and Nanobelts. *Chem. Mater.* **2006**, *18*, 547−553.
(19) Huang, M.; Zhang, Y.; Li, F.; Zhang, L.; Ruoff, R. S.; Wen, Z.; Liu, Q. Self-Assembly of Mesoporous Nanotubes Assembled from Interwoven Ultrathin Birnessite-Type MnO_2 Nanosheets for Asymmetric Supercapacitors. *Sci. Rep.* **2014**, *4*, 3878.
(20) Chen, J. Recent Progress in Advanced Materials for Lithium Ion Batteries. *Materials* **2013**, *6*, 156−183.
(21) Zhu, Y. R.; Ji, X. B.; Pan, C. C.; Sun, Q. Q.; Song, W. X.; Fang, L. B.; Chen, Q. Y.; Banks, C. E. A Carbon Quantum Dot Decorated RuO_2 Network: Outstanding Supercapacitances under Ultrafast Charge and Discharge. *Energy Environ. Sci.* **2013**, *6*, 3665−3675.
(22) Barranco, V.; Pico, F.; Ibanez, J.; Lillo-Rodenas, M. A.; Linares-Solano, A.; Kimura, M.; Oya, A.; Rojas, R. M.; Amarilla, J. M.; Rojo, J. M. Amorphous Carbon Nanofibres Inducing High Specific Capacitance of Deposited Hydrous Ruthenium Oxide. *Electrochim. Acta* **2009**, *54*, 7452−7457.
(23) Wu, Z. S.; Wang, D. W.; Ren, W.; Zhao, J.; Zhou, G.; Li, F.; Cheng, H. M. Anchoring Hydrous RuO_2 on Graphene Sheets for High-Performance Electrochemical Capacitors. *Adv. Funct. Mater.* **2010**, *20*, 3595−3602.
(24) Miller, J. M.; Dunn, B.; Tran, T. D.; Pekala, R. W. Deposition of Ruthenium Nanoparticles on Carbon Aerogels for High Energy Density Supercapacitor Electrodes. *J. Electrochem. Soc.* **1997**, *144*, L309−L311.
(25) Zheng, J. P. Ruthenium Oxide-Carbon Composite Electrodes for Electrochemical Capacitors. *Electrochem. Solid-State Lett.* **1999**, *2*, 359−361.
(26) Kim, J. Y.; Kim, K. H.; Yoon, S. B.; Kim, H. K.; Park, S. H.; Kim, K. B. In Situ Chemical Synthesis of Ruthenium Oxide/Reduced Graphene Oxide Nanocomposites for Electrochemical Capacitor Applications. *Nanoscale* **2013**, *5*, 6804−6811.
(27) Applestone, D.; Manthiram, A. Cu_6Sn_5-TiC-C Nanocomposite Alloy Anodes with High Volumetric Capacity for Lithium Ion Batteries. *RSC Adv.* **2012**, *2*, 5411−5417.
(28) Yuan, C. Z.; Li, J. Y.; Hou, L. R.; Yang, L.; Shen, L. F.; Zhang, X. G. Facile Template-Free Synthesis of Ultralayered Mesoporous Nickel Cobaltite Nanowires towards High-Performance Electrochemical Capacitors. *J. Mater. Chem.* **2012**, *22*, 16084−16090.
(29) Santhanagopalan, S.; Balram, A.; Meng, D. D. Scalable High-Power Redox Capacitors with Aligned Nanoforests of Crystalline MnO_2 Nanorods by High Voltage Electrophoretic Deposition. *ACS Nano* **2013**, *7*, 2114−2125.
(30) Aricò, A. S.; Bruce, P.; Scrosati, B.; Tarascon, J. M.; Van Schalkwijk, W. Nanostructured Materials for Advanced Energy Conversion and Storage Devices. *Nat. Mater.* **2005**, *4*, 366−377.
(31) Liu, J.; Cao, G. Z.; Yang, Z. G.; Wang, D. H.; Dubois, D.; Zhou, X. D.; Graff, G. L.; Pederson, L. R.; Zhang, J. G. Oriented Nanostructures for Energy Conversion and Storage. *ChemSusChem* **2008**, *1*, 676−697.
(32) Liu, N.; Lu, Z. D.; Zhao, J.; McDowell, M. T.; Lee, H. W.; Zhao, W. T.; Cui, Y. A Pomegranate-Inspired Nanoscale Design for Large-Volume-Change Lithium Battery Anodes. *Nat. Nanotechnol.* **2014**, *9*, 187−192.
(33) Weng, Z.; Guo, H.; Liu, X.; Wu, S.; Yeung, K. W. K.; Chu, P. K. Nanostructured TiO_2 for Energy Conversion and Storage. *RSC Adv.* **2013**, *3*, 24758−24775.
(34) Li, Y. L.; Wang, J. J.; Zhang, Y.; Banis, M. N.; Liu, J.; Geng, D. S.; Li, R. Y.; Sun, X. L. Facile Controlled Synthesis and Growth Mechanisms of Flower-like and Tubular MnO_2 Nanostructures by Microwave-Assisted Hydrothermal Method. *J. Colloid Interface Sci.* **2012**, *369*, 123−128.
(35) Wang, C.; Zhou, Y.; Ge, M.; Xu, X.; Zhang, Z.; Jiang, J. Z. Large-Scale Synthesis of SnO_2 Nanosheets with High Lithium Storage Capacity. *J. Am. Chem. Soc.* **2010**, *132*, 46−47.
(36) Jiang, H.; Sun, T.; Li, C. Z.; Ma, J. Hierarchical Porous Nanostructures Assembled from Ultrathin MnO_2 Nanoflakes with Enhanced Supercapacitive Performances. *J. Mater. Chem.* **2012**, *22*, 2751−2756.
(37) Chen, Q.; Zhou, W. Z.; Du, G. H.; Peng, L. M. Tritanate Nanotubes Made via a Single Alkali Treatment. *Adv. Mater.* **2002**, *14*, 1208−1211.
(38) Ma, R. Z.; Sasaki, T. Nanosheets of Oxides and Hydroxides: Ultimate 2D Charge-Bearing Functional Crystallites. *Adv. Mater.* **2010**, *22*, 5082−5104.
(39) Zheng, J. P.; Cygan, P. J.; Jow, T. R. Hydrous Ruthenium Oxide as an Electrode Material for Electrochemical Capacitors. *J. Electrochem. Soc.* **1995**, *142*, 2699−2703.
(40) Cho, S.; Liu, L. C.; Yoo, S. H.; Jang, H. Y.; Park, S. Template-Assisted Electrochemical Growth of Hydrous Ruthenium Oxide Nanotubes. *Bull. Korean Chem. Soc.* **2013**, *34*, 1462−1467.
(41) Kim, J. Y.; Kim, K. H.; Kim, H. K.; Park, S. H.; Chung, K. Y.; Kim, K. B. Nanosheet-Assembled 3D Nanoflowers of Ruthenium Oxide with Superior Rate Performance for Supercapacitor Applications. *RSC Adv.* **2014**, *4*, 16115−16120.
(42) Connick, R. E.; Hurley, C. R. Chemistry of Ru (VI),-(VII) and-(VIII). Reactions, Oxidation Potentials and Spectra. *J. Am. Chem. Soc.* **1952**, *74*, 5012−5015.
(43) Kim, W. H.; Park, S. J.; Kim, D. Y.; Kim, H. Atomic Layer Deposition of Ruthenium and Ruthenium-oxide Thin Films by Using a Ru(EtCp)(2) Precursor and Oxygen Gas. *J. Korean Phys. Soc.* **2009**, *55*, 32−37.
(44) Mun, C.; Ehrhardt, J.; Lambert, J.; Madic, C. XPS Investigations of Ruthenium Deposited onto Representative Inner Surfaces of Nuclear Reactor Containment Buildings. *Appl. Surf. Sci.* **2007**, *253*, 7613−7621.
(45) Nakahira, A.; Kubo, T.; Numako, C. Formation Mechanism of TiO_2-Derived Titanate Nanotubes Prepared by the Hydrothermal Process. *Inorg. Chem.* **2010**, *49*, 5845−5852.
(46) Wang, B.; Li, X. L.; Qiu, T. F.; Luo, B.; Ning, J.; Li, J.; Zhang, X. F.; Liang, M. H.; Zhi, L. J. High Volumetric Capacity Silicon-Based Lithium Battery Anodes by Nanoscale System Engineering. *Nano Lett.* **2013**, *13*, 5578−5584.
(47) Che, G.; Lakshmi, B. B.; Fisher, E. R.; Martin, C. R. Carbon Nanotubule Membranes for Electrochemical Energy Storage and Production. *Nature* **1998**, *393*, 346−349.
(48) Choi, J. W.; Hu, L.; Cui, L.; McDonough, J. R.; Cui, Y. Metal Current Collector-Free Freestanding Silicon-Carbon 1D Nanocomposites for Ultralight Anodes in Lithium Ion Batteries. *J. Power Sources* **2010**, *195*, 8311−8316.
(49) Vlad, A.; Reddy, A. L. M.; Ajayan, A.; Singh, N.; Gohy, J. F.; Melinte, S.; Ajayan, P. M. Flexible Lithium-Polymer Batteries with Cu@Si Core-Shell Nanowire Composites Anodes. *Proc. Natl. Acad. Sci. U. S. A.* **2012**, *109*, 15168−15173.
(50) Taberna, P. L.; Mitra, S.; Poizot, P.; Simon, P.; Tarascon, J. M. High Rate Capabilities Fe_3O_4-Based Cu Nano-Architectured Electrodes for Lithium-Ion Battery Applications. *Nat. Mater.* **2006**, *5*, 567−573.
(51) Zhang, S. C.; Du, Z. J.; Lin, R. X.; Jiang, T.; Liu, G. R.; Wu, X. M.; Weng, D. S. Nickel Nanocone-Array Supported Silicon Anode for High-Performance Lithium-Ion Batteries. *Adv. Mater.* **2010**, *22*, 5378−5382.
(52) Bhaskar, S.; Dobal, P. S.; Majumder, S. B.; Katiyar, R. S. X-Ray Photoelectron Spectroscopy and Micro-Raman Analysis of Conductive RuO_2 Thin Films. *J. Appl. Phys.* **2001**, *89*, 2987−2992.
(53) Lee, S. H.; Liu, P.; Cheong, H. M.; Tracy, C. E.; Deb, S. K. Electrochromism of Amorphous Ruthenium Oxide Thin Films. *Solid State Ionics* **2003**, *165*, 217−221.
(54) Jo, H. C.; Kim, K. M.; Cheong, H.; Lee, S. H.; Deb, S. K. In Situ Raman Spectroscopy of RuO_2 Center Dot xH_2O. *Electrochem. Solid-State Lett.* **2005**, *8*, E39−E41.
(55) Foelske, A.; Barbieri, O.; Hahn, M.; Kotz, R. An X-Ray Photoelectron Spectroscopy Study of Hydrous Ruthenium Oxide Powders with Various Water Contents for Supercapacitors. *Electrochem. Solid-State Lett.* **2006**, *9*, A268−A272.
(56) Sato, Y.; Yomogida, K.; Nanaumi, T.; Kobayakawa, K.; Ohsawa, Y.; Kawai, M. Electrochemical Behavior of Activated-Carbon Capacitor

DOI: 10.1021/acsami.5b04360
ACS Appl. Mater. Interfaces 2015, 7, 16686−16693

Materials Loaded with Ruthenium Oxide. *Electrochem. Solid-State Lett.* **2000**, *3*, 113−116.
(57) Campbell, P.; Ortner, M.; Anderson, C. Differential Thermal Analysis and Thermogravimetric Analysis of Fission Product Oxides and Nitrates to 1500 C. *Anal. Chem.* **1961**, *33*, 58−61.
(58) Kim, H.; Popov, B. N. Characterization of Hydrous Ruthenium Oxide/Carbon Nanocomposite Supercapacitors Prepared by a Colloidal Method. *J. Power Sources* **2002**, *104*, 52−61.
(59) McKeown, D. A.; Hagans, P. L.; Carette, L. P. L.; Russell, A. E.; Swider, K. E.; Rolison, D. R. Structure of Hydrous Ruthenium Oxides: Implications for Charge Storage. *J. Phys. Chem. B* **1999**, *103*, 4825−4832.
(60) Chen, L. Y.; Hou, Y.; Kang, J. L.; Hirata, A.; Fujita, T.; Chen, M. W. Toward the Theoretical Capacitance of RuO_2 Reinforced by Highly Conductive Nanoporous Gold. *Adv. Energy Mater.* **2013**, *3*, 851−856.

DOI: 10.1021/acsami.5b04360
ACS Appl. Mater. Interfaces 2015, 7, 16686−16693